
Article:
Gawthrop, P.J., Wallace, M.I. and Wagg, D.J. (2005) Bond-graph based substructuring of dynamical systems. Earthquake Engineering and Structural Dynamics., 34 (6). 687 - 703. ISSN: 0098-8847

https://doi.org/10.1002/eqe.450

Bond-graph Based Substructuring of Dynamical Systems

P. J. Gawthrop[1,*], M. I. Wallace[2] and D. J. Wagg[2]

[1] *Centre for Systems and Control and Department of Mechanical Engineering, University of Glasgow, GLASGOW. G12 8QQ UK*

[2] *Department of Mechanical Engineering, Queens Building, University of Bristol, Bristol BS8 1TR, UK.*

SUMMARY

A bond graph approach to hybrid simulation of dynamical systems using numerical-experimental real-time substructuring is presented. The bond graph concepts of a *virtual junction* and a *virtual actuator*, hitherto used in the context of physical-model based control, are used to perform the substructuring in an intuitively appealing way. The approach is illustrated by the reworking of a previously-published example.

The approach is verified experimentally using a bench-top multiple mass-spring system for the physical substructure and automatically generated real-time code is used to implement the numerical substructure.

KEY WORDS: Numerical-experimental substructuring; bond graphs; real-time control.

*Correspondence to: P. .J .Gawthrop, Centre for Systems and Control and Department of Mechanical Engineering, University of Glasgow, GLASGOW. G12 8QQ UK. **P.Gawthrop@eng.gla.ac.uk**

1. Introduction

This paper brings together two hitherto disparate research areas: real-time numerical-experimental substructure-based testing of structures under dynamic loading as discussed by Wagg and Stoten [1] and Darby et al. [2]; and bond graph based physical-model-based control as introduced by Sharon et al. [3] and extended by Gawthrop [4], Costello and Gawthrop [5] and, in particular the *virtual actuator* approach of Gawthrop *et.al.* [6, 7].

Real-time dynamic substructuring is a novel experimental testing technique which can be used to test individual components of engineering systems. This type of testing has been developed from experimental testing of large scale structures using multiple time scales [8, 9]. The basic concept is that a complete model of the system is made by combining an experimental part with a numerical part. Originally this was done for situations where numerical models of the experimental part were unreliable — such as failure of concrete columns under earthquake loading [10]. However, the technique has now been developed for a broader range of applications and in fact can now also be viewed as an advanced form of component testing. In the fields of mechanical and aerospace engineering, physical components are often tested to either characterise or improve the design performance. Substructure testing offers a way of accurately testing nonlinear components which can be useful in many applications in these fields. Some examples are described in [11] in connection with aerospace engineering. To carry out a substructuring test the component of interest is isolated and fixed into an experimental test system. To link the experimental substructure to the numerical substructure, a set of *transfer systems* are controlled to follow the appropriate output from the numerical model. At the same time the forces between the transfer systems and experimental substructure are fed back into the numerical model to give a form bi-directional coupling. The key challenge is to carry out this operation effectively in real time [1, 12, 2, 13]. The issue of the level of accuracy achieved by the substructuring process is also a critical

issue [14].

The bond graph approach to modelling of dynamic systems, introduced by Henry Paynter of MIT [15], is well established [16, 17, 18, 19, 20, 21]. The authors believe that the approach provides a natural conceptual framework for reasoning about substructuring.

As noted by Wagg and Stoten [1], the key issue of substructuring to be resolved is the *synchronisation* of the motion of the *physical substructure* and the computer-based *numerical substructure*. There are two distinct problems here: the fact that the numerical integration implicit in the numerical substructure introduces errors and the fact that there is usually a dynamical system (the *transfer system*) interposed between the computer and the physical systems. In this paper, the former is referred to as the *numerical synchronisation* problem and the latter as the *physical synchronisation* problem. The *numerical synchronisation* problem is essentially an issue of numerical analysis. It has been discussed by, for example, Darby et al. [2] and Algaard et al. [22]. Although important, it is not the subject of this paper.

The physical synchronisation is essentially a control problem, with the response delay of the actuator being the critical issue for the substructuring algorithm. Delay compensation is a well known issue for real-time substructuring, with a number of single step forward prediction approaches having already been presented by Horiuchi et al. [23], Darby et al. [13] along with other compensation techniques such as Horiuchi and Konno [24] which have shown to improve accuracy. A more generic approach is presented by Wallace et al. [14] which allows multiple and fractions of one time step to be predicted without interpolation. Given the insight afforded by the bond graph approach, this paper shows that an alternative solution to the physical synchronisation problem is provided by the *virtual actuator* approach of Gawthrop *et.al.* [6, 7]. This method has the advantage that the virtual junction will provide compensation of transfer-system dynamics for all frequency ranges. Additionally, this approach can,

in principle, be used in the case when the substructure is nonlinear. However, within the context of this paper, the virtual junction approach is applied to linear substructured systems.

The paper is organised as follows. Section 2 gives a bond graph based interpretation of substructuring. Section 3 introduces virtual junctions and actuators and section 4 illustrates the method using a previously used example [1]. Section 5 discusses an experimental verification of the approach, and Section 6 concludes the paper and discusses some possible extensions.

2. Bond Graph Substructuring

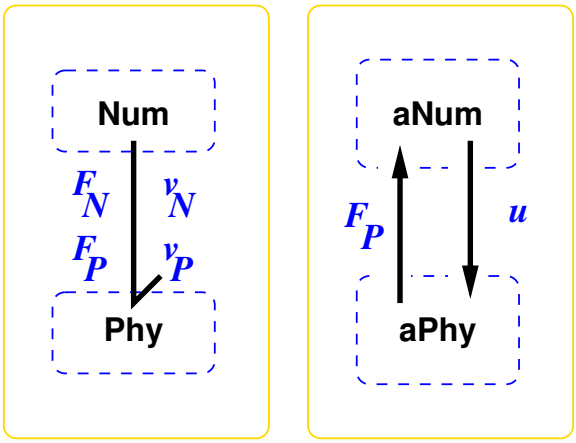

(a) Model (b) Augmented Model

Figure 1. Substructuring

Following Wagg and Stoten [1] and Darby et al. [2], this paper considers *real-time dynamic* substructuring whereby a dynamic system is *substructured* into two parts:

numerical substructure to be simulated numerically and

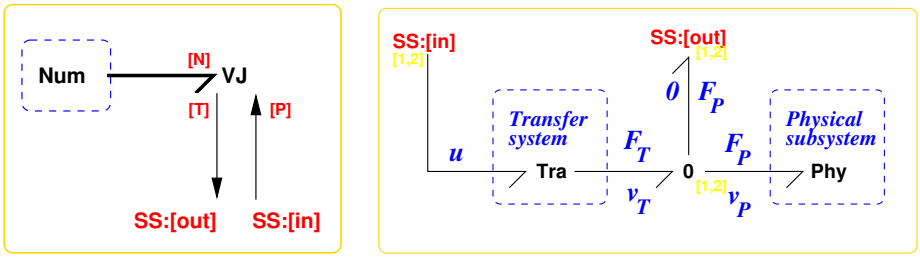

(a) Numerical (b) Physical

Figure 2. Augmented substructures

physical substructure to be implemented physically.

Substructuring can be readily described in bond graph terms as follows. Given the bond graph of a dynamic system, choose the set of components forming the physical substructure and mark all bonds external to this substructure, in general there will be $N \geq 1$ such bonds and the remaining components will form the numerical substructure. Thus each of the two substructures has N ports connected by the N marked bonds. In the case of mechanical systems, each port will correspond to a force-velocity pair; in general this can be any effort-flow pair.

This decomposition is depicted in Figure 1(a) where **Num** and **Phy** are the numerical and physical substructures respectively. F_N and v_N are the force/velocity pair associated with the numerical substructure and F_P and v_P are the force/velocity pair associated with the physical substructure. The connecting bond implements the two *interface equations*:

$$\begin{cases} F_P &= F_N \\ v_P &= v_N \end{cases} \tag{1}$$

The energy bond of Figure 1(a) will, in general, be a *vector* bond corresponding to N scalar bonds

and thus both the numerical and physical substructures may themselves contain many subsystems. In this case, the quantities in (1) can be regarded as vectors containing N components. The simulation example of Section 4 has $N = 1$; the experimental example of Section 5 has $N = 2$.

As pointed out previously, [1, 2] it is often not possible to connect the two substructures of Figure 1(a) because it is not physically possible to directly apply the signal implied by the numerical substructure to the physical system. In bond graph terms, the two systems of Figure 1(a) *cannot* be connected via an energy bond; as indicated in Figure 1(b), *augmented* versions of the numerical (**aNum**) and physical (**aPhy**) substructure are connected using a pair of active bonds. For the purposes of this paper it is assumed that:

Assumption 1. *The causality is such that the* physical *substructure in Figure 1(a) imposes a* force *(in general effort) on the* numerical *substructure.*

Assumption 2. *The quantity imposed by the* physical *substructure in Figure 1(a) can be directly measured.*

Assumption 3. *The quantity imposed by the* numerical *substructure of Figure 1(a) cannot be directly imposed on the* physical *substructure but rather via an N-input u* transfer system*. In particular, the input u can only be imposed via a* transfer system *labelled **Tra** in Figure 2(b).*

Assumption 1 is not essential but simplifies the development; assumption 2 is essential for this paper but could be removed as discussed in Section 6; assumption 3 is the main issue addressed here.

The fact that the substructured system of Figure 1(a) cannot be directly implemented but rather must be approximated by Figure 1(b) means that (1) no longer holds and must be replaced by:

$$\begin{cases} F_P - F_N & = \tilde{F} \\ v_P - v_N & = \tilde{v} \end{cases} \tag{2}$$

where $\tilde{F}$ is the *force synchronisation error* and $\tilde{v}$ is the *velocity synchronisation error*. The synchronisation problem is to reduce the two synchronisation errors to acceptable values; *exact synchronisation*[†] corresponds to

$$\begin{cases} \tilde{F} & = 0 \\ \tilde{v} & = 0 \end{cases} \tag{3}$$

A similar problem has been noted in the context of bond graph based physical-model based control [6, 7]. This paper applies the (suitably modified) solution of this control problem to the substructuring problem. In particular, it is shown constructively in Section 3 that if the augmented *physical* substructure **aPhy** of Figure 1(b) is given by Figure 2(a), then the three-port (each port corresponding to N bonds) virtual junction **VJ** component can, in certain circumstances, provide a solution to the *exact synchronisation* problem.

3. Virtual junctions and Actuators

The *virtual actuator* approach to control system design was introduced by Gawthrop et al. [6] and experimentally verified by [7] in the context of control system design. The same concepts are used in this paper in the context of substructuring; this section gives a brief overview of the approach.

The virtual junction component appearing in Figure 1(b) has three ports labelled:

[P], carrying the measured signal y from the *physical* system but imposing 0 signal onto the physical system;

[T], carrying the control signal u to the input of the *transfer* system but not carrying any measurement

[†]In fact, there are many possible definitions of synchronisation analogous to the many definitions of stability.

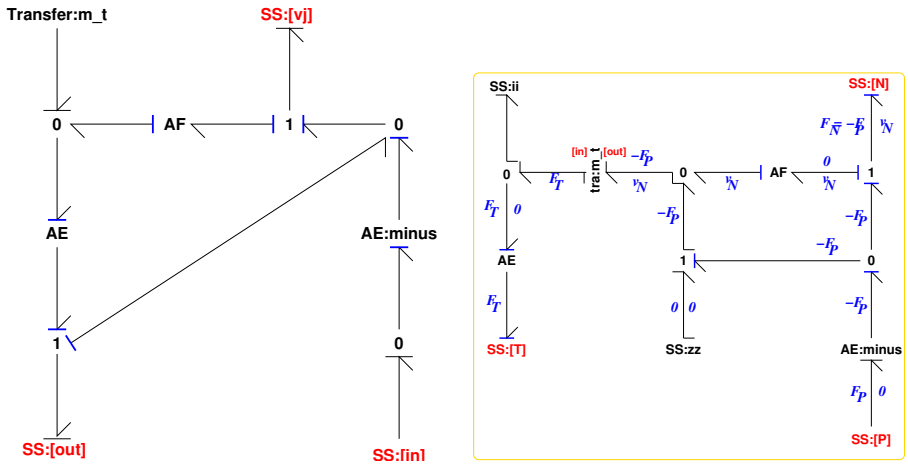

(a) Collocated (b) Non-collocated

Figure 3. Virtual Junction: bond graph

and

[N] the port to which the numerical system is attached.

The purpose of the virtual junction is to make the input-output properties of the systems of Figure 1(a) and 1(b) identical. For example, this can be done if the virtual junction implements the equations:

$$\begin{pmatrix} F_N \\ F_T \end{pmatrix} = \begin{pmatrix} -1 & 0 \\ 1 & T^{-1} \end{pmatrix} \begin{pmatrix} F_P \\ v_N \end{pmatrix} \tag{4}$$

where $v_T = TF_T$.

The design of the virtual junction component is considered in detail elsewhere [7, 6]. The design for a particular example is discussed in Section 4. Given the structure of Figure 1, there are two restrictions on the class of systems for which a virtual junction can be successfully implemented:

Assumption 4. *The transfer system is stable and has stable zero dynamics.*

Assumption 5. *Defining* σ_N *as the length of the shortest causal path (SCP) between* F_N *and* v_N *and* σ_T *as the length of the SCP between* F_T *and* v_T*, then:*

$$\sigma_N \geq \sigma_T \tag{5}$$

Assumption 4 ensures internal stability and assumption 5 ensures that the combined numerical substructure and virtual junction is proper and thus has a state-space realisation.

It is clear from this that an accurate model of the *transfer* system is required. Section 5 has more discussion on this point.

4. Simulation Example

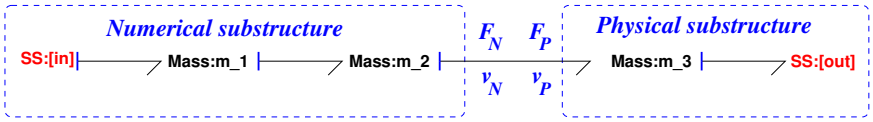

(a) Three-mass system: bond graph

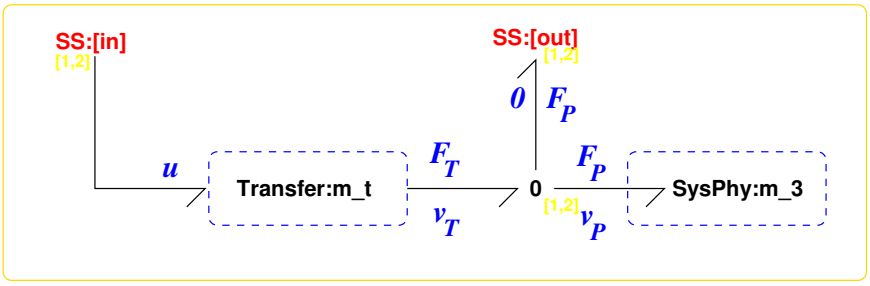

(b) Physical system: bond graph

Figure 4. Example: Desired and Physical systems

Figure 5. Example: transfer system

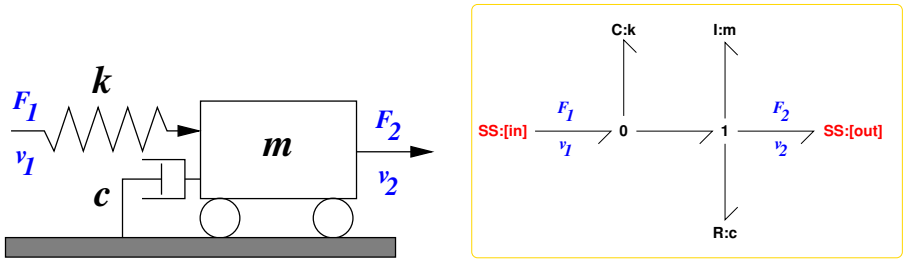

(a) Schematic (b) Bond graph

Figure 6. Mass-spring-damper System

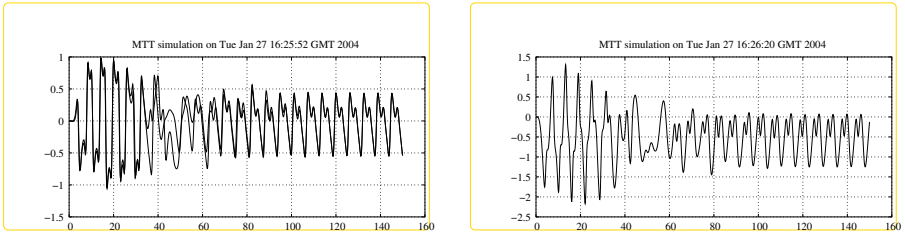

(a) Simulation: desired response y_d and substructured output y_s

(b) Simulation: control signal u

Figure 7. Example: Simulation results. $m_1 = m_2 = m_3 = m_t = 1$, $c_1 = c_2 = c_3 = 0.1$, $c_t = 1$, $k_1 = k_2 = k_t = 1$, $k_3 = -1 + \delta^2$ where δ is the spring extension. $r = -0.5\sin(t)$

Wagg and Stoten [1] consider substructuring in the context of a three mass-spring-damper system equivalent to that shown as a bond graph in Figure 4(a). The **Mass** components labelled m_1–m_3 are

three instances of the **Mass** component depicted in Figure 6. In the example of Wagg and Stoten [1] , the third mass (m_3 in Figure 4) is a physical system whereas the other two masses (m_1 & m_2 in Figure 4) are to be realised by numerical simulation. Causal strokes have been added to show that, in this case, Assumption 1 holds.

Further, with reference to Figure 4(b) the physical mass m_3 is controlled via the *transfer system* m_t. As shown in Figure 5, the **Transfer** system is based on the **Mass** substructure with the left-hand port connected to a zero velocity source. This gives a simpler situation than that of Figure 1 as both F_T and v_T are associated with a single port.

Following the approach of Section 2, the numerical system is obtained as in Figure 2(a) by attaching the masses m_1 & m_2 to the *virtual junction* which is shown in expanded form in 3(a). The virtual junction transfer function representation is:

$$\begin{pmatrix} F_N \\ F_T \end{pmatrix} = \begin{pmatrix} -1 & 0 \\ 1 & \frac{(c_t s + k_t + m_t s^2)}{s} \end{pmatrix} \begin{pmatrix} F_P \\ V_N \end{pmatrix} \tag{6}$$

The overall system then consists of the *numerical* and *physical* systems connected as in Figure 1. As discussed in Section 2, the numerical simulation corresponds to a *proper* transfer function. The corresponding state-space matrices are:

$$A = \begin{pmatrix} 0 & \frac{(-1)}{m_1} & 0 & 0 & 0 \\ k_1 & \frac{(-c_1)}{m_1} & -k_2 & 0 & 0 \\ 0 & \frac{1}{m_1} & 0 & \frac{(-1)}{m_2} & 0 \\ 0 & 0 & k_2 & \frac{(-c_2)}{m_2} & 0 \\ 0 & 0 & 0 & \frac{1}{m_2} & 0 \end{pmatrix} \tag{7}$$

$$B = \begin{pmatrix} 0 & 1 \\ 0 & 0 \\ 0 & 0 \\ -1 & 0 \\ 0 & 0 \end{pmatrix} \tag{8}$$

$$C = \begin{pmatrix} 0 & 0 & \frac{(k_2 m_t)}{m_2} & \frac{(-c_2 m_t + c_t m_2)}{m_2^2} & k_t \end{pmatrix} \tag{9}$$

$$D = \begin{pmatrix} \frac{(m_2 - m_t)}{m_2} & 0 \end{pmatrix} \tag{10}$$

The desired system of Figure 4(a) and the substructured system of Figure 1 were both simulated using the numerical parameters indicated in Figure 7 and the velocity of the third mass of the desired system (y_d), together with the corresponding velocity of the third mass of the substructured system (y_s), are plotted in Figure 7(a). There is a transient error due to a non-zero initial condition being applied to the transfer system (initial velocity = 0.01). With zero initial conditions, $y_s = y_d$. Figure 7(b) shows the control signal associated with the substructured system: the external force applied to the transfer system. The simulation code was automatically generated from the bond graph diagrams using MTT [25].

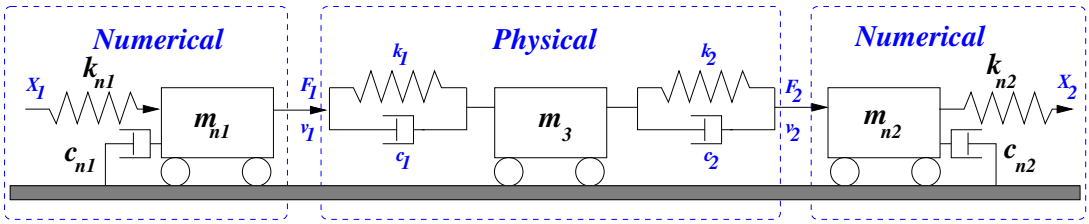

Figure 8. Physical/Numerical Substructured system. $k_{n1} = k_{n2} = k_1 = k_2 = 4750\text{Nm}^{-1}$; $c_{n1} = c_{n2} = c_1 = c_2 = 6\text{Nsm}^{-1}$; $m_{n1} = m_{n2} = m_3 = 6\text{Nsm}^{-1}$.

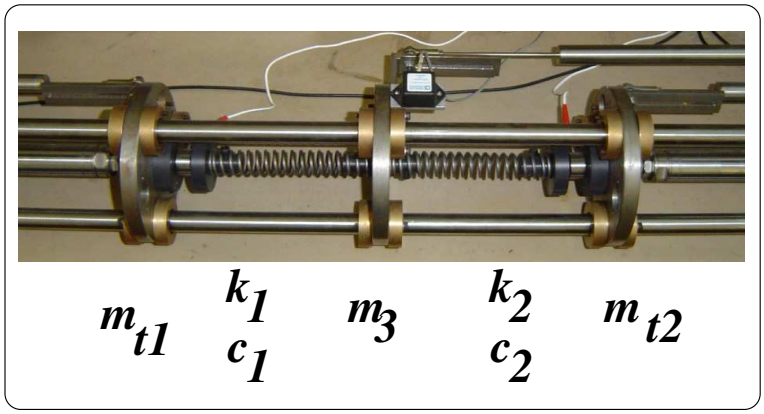

Figure 9. Augmented Physical substructure: Photo

5. Experimental Example

The model to be simulated appears in Figure 8; it has been divided into physical and numerical substructures and the parameters are given in the caption. The physical substructure is modelled as Figure 10. Thus the substructured model corresponding to this example appears in Figure 1(a) where both the numerical and physical substructures have been vectorised with $N = 2$.

Figure 9 shows the substructured three mass system. The physical substructure is the central mass m_3 of Figure 9 together with two attached springs. A load cell is inserted between the mass m_{t1} and the

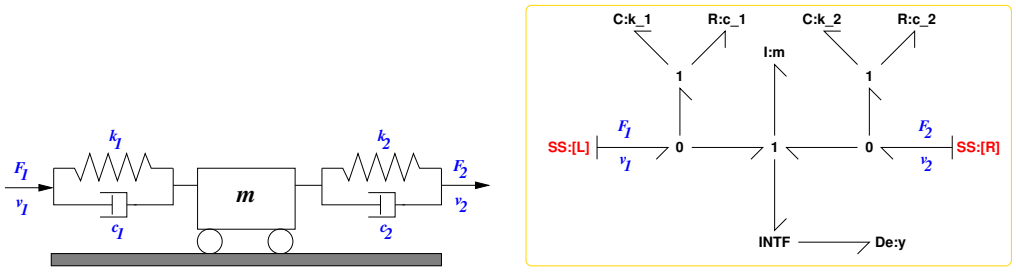

(a) Schematic (b) Bond graph

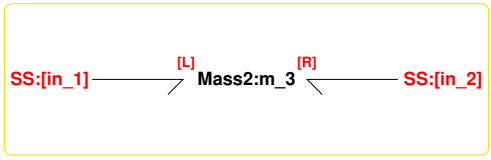

(c) Vector bond graph

Figure 10. A two-port system

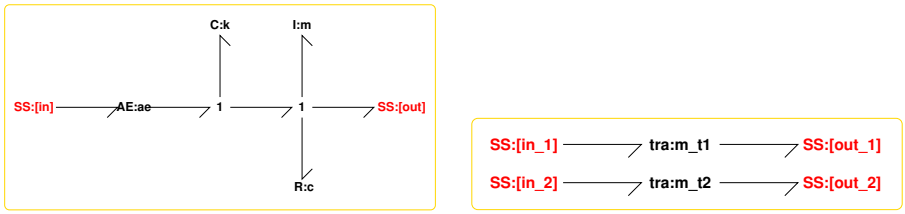

(a) **tra** component bond graph (b) Bond graph

Figure 11. Experimental example: Transfer system (**Tra**)

spring k_1 and another between the mass m_{t2} and the spring k_2. The left-hand mass m_{t1}, together with the actuator, forms the scalar transfer system **tra** of Figure 11(a); two instances of **tra** are combined in Figure 11(b) to form the vector transfer system **Tra**.

To implement real-time substructuring we are using a dSpace DS1104 R&D Controller Board running on hardware architecture of MPC8240 (PowerPC 603e core) at 250 MHz with 32 MB synchronous DRAM (SDRAM). This DSP type board offers 4 A/D channels at 16 bit, 4 A/D channels at 12 bit with 8 D/A channels at 16 bit, of which 5 and 4 are required respectively for this substructuring example. This is fully integrated into the block diagram-based modelling tool MATLAB™/Simulink™which is used to build the substructuring model. The dSpace companion software ControlDesk is used for online analysis and control, providing soft real-time access to the hard real-time application.

Simulink™s-functions were automatically generated from the bond graph representation of the augmented numerical substructure **aNum** of Figures 1(b) and 2(a) using the MTT [25] package.

Two UBA (timing belt and ball screw configuration) linear Servomech actuators are used as the transfer systems, with maximum force capacity of 500N and maximum linear speed of 640mms^{-1}. These are driven independently by two Panasonic Minas Series AC servo motors which are configured as analogue amplifiers to remove any internal closed loop control functions. Three RDP Electronics DCT captive guided DC LVDT displacement transducers are used to measure the displacement of the two transfer systems and the substructure which have a $\pm 0.11\%$ linearity error on full scale deflection of 50mm. Each unit has an internal bearing that guides the armature built-in DC to DC signal conditioning to help remove noise. Two RDP Electronics model 31 precision miniature tension/compression load cells are used for the force measurements either side of the substructure. The unit is applicable both in tension and compression with linearity $\pm 0.15\%$, hysteresis $\pm 0.15\%$ and non-repeatability $\pm 0.1\%$ of full scale deflection. Each mass is a constant 2.2kg and connected to the rig via three parallel shafts constraining their motion to one degree of freedom with an axial alignment accuracy of ± 0.1mm. Each mass has three LBBP linear ball bearings with double lip seals and raceway

plates to reduce friction. Through system identification the spring constants were found constant for all and equal to $k = 4750\text{Nm}^{-1}$ and damping ratio of $c = 6\text{Nsm}^{-1}$.

There were two sets of experiments: identification of a dynamical model of the transfer system (Section 5.1) and validation of the bond graph approach to substructuring (Section 5.2).

5.1. Transfer system identification

The left-hand transfer system has the following components:

1. the linear actuator, comprising an AC servo motor and associated power amplifier driving a ball-screw mechanism;
2. the mass m_{t1} of Figure 9, equal to 2.2 kg;
3. the LVDT sensor measuring the position x_1 of the mass m_{t1}

The right-hand transfer system was similar.

As discussed in section 3, the virtual junction approach requires an accurate model of the transfer system. Unfortunately, AC servos are non-linear [26] and difficult to characterise from first principles as is the ball screw mechanism. Analysis of experimental measurements of step responses showed that the dynamical response of the servo motor/ball-screw was indeed dependent on the form of the input signal.

Most actuators used in this context are indeed non-linear and this must therefore be an important consideration in transfer system design. In particular, it is well-known that the use of feedback reduces uncertainly and nonlinearity. For this reason, a variable-gain proportional digital controller with gain g_1, sample interval $\Delta = 1\text{ms}$, setpoint x_{d1} and described by

$$u_1 = g_1 \left(x_{d1} - x_1 \right) \tag{11}$$

was implemented where u_1 is the input to the linear actuator 1. The *closed-loop* transfer system was observed to have a more linear response than the open-loop transfer system.

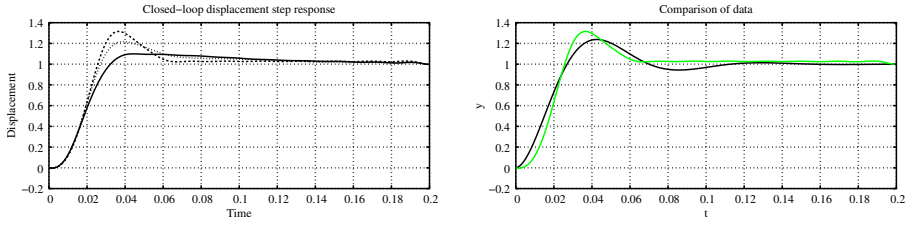

(a) x_{t1} for $g_1 = 0.6, 0.8, 1.0$ (b) x_{t1}&$\hat{x}_{t1}$ for $g_1 = 1.0$

Figure 12. Identified transfer system step responses

Name	Value
c_{t1}	150.8
k_{t1}	13618.0
c_{t2}	200.8
k_{t2}	25902.0

Table I. Estimated Parameters

Sequences of input (x_{d1}) and output (x_1) data were measured when the mass was disconnected from the spring k_1 for three values of g_1. Using the "frequency-sampling filter" method of Wang and Cluett [27], a step response (relating x_{d1} and x_1) was identified for each of the three values of gain and plotted in Figure 12(a). Although the bond graph of Figure 11 does not correspond in detail to the actual transfer system, it is *physically plausible* in the sense of Gawthrop [28] and so its parameters can be estimated using the **sensitivity** bond graph approach [29]. The mass m_{t1} is known, and so the two remaining parameters (spring stiffness k_{t1} and damping c_{t1} are identified and appear in Table I. We

must repeat this identification for the right hand transfer system as its frictional characteristics are not necessarily the same regardless of its mechanical similarity. In fact it can be seen from Table I that the dynamics from Transfer System 2 are quite different.

The step responses of this physically plausible model are compared with the data-based step response of 12(a) for $g_1 = 1.0$ in Figure 12(b). The match is not perfect, but the identified model was used for the experiments of Section 5.2.

5.2. Experimental validation

Synchronisation subspace plots are used to show the effectiveness of the control algorithm by plotting the desired verses actual responses, [30]. A subspace plot shows the amplitude accuracy and the magnitude of delay coupled together at any one time interval. Perfect synchronisation is represented by a straight line at an angle of 45° to the horizontal with maxima and minima of the reference signal. Any reduction in synchronisation can be seen as a deviation from this idealised line. The result of varying the amplitude accuracy is to change the angular orientation of the subspace plot compared to the idealised line whereas a constant delay between the reference signal and the response results in transforming the idealised straight line into an ellipse.

For constant wall excitation conditions these plots builds up into a repeating periodic pattern, which can appear complex. However, the individual components of amplitude and delay produce their own specific and identifiable patterns if evaluated separately. We use subspace plots as they allow the controller effectiveness to be characterised in an online procedure, important for real-time testing, and displays far more information than can be interpreted from simply observing the error between the two signals.

First, we investigate the case where the wall excitations are equal and opposite. To achieve

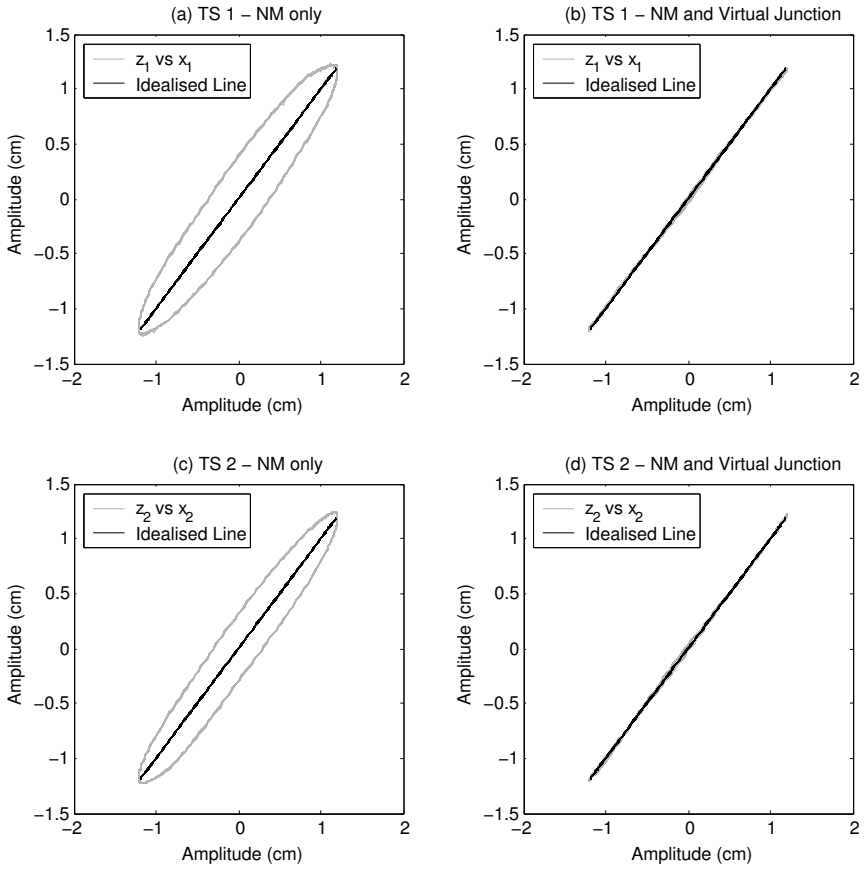

Figure 13. Wall excitation of $r_1 = 5Hz$ and $r_2 = 5Hz$.

synchronisation, the *actual* displacement of the transfer system, x_i, must be equal to the *desired* output from its respective numerical model (NM), z_i, where $i = 1,2$ according to the transfer system being observed. Figure 13 shows the results of both transfer systems for a sinusoidal excitation of $5Hz$ from each wall, r_1 and r_2. We compare the effectiveness of the control algorithm when the virtual junction is included in the numerical model, (b) and (d), to when there is no plant model included, (a) and (c). We can clearly see that the constant phase delay caused by the mechanical characteristics of each transfer system has been effectively removed by the inclusion of the virtual junction in both transfer

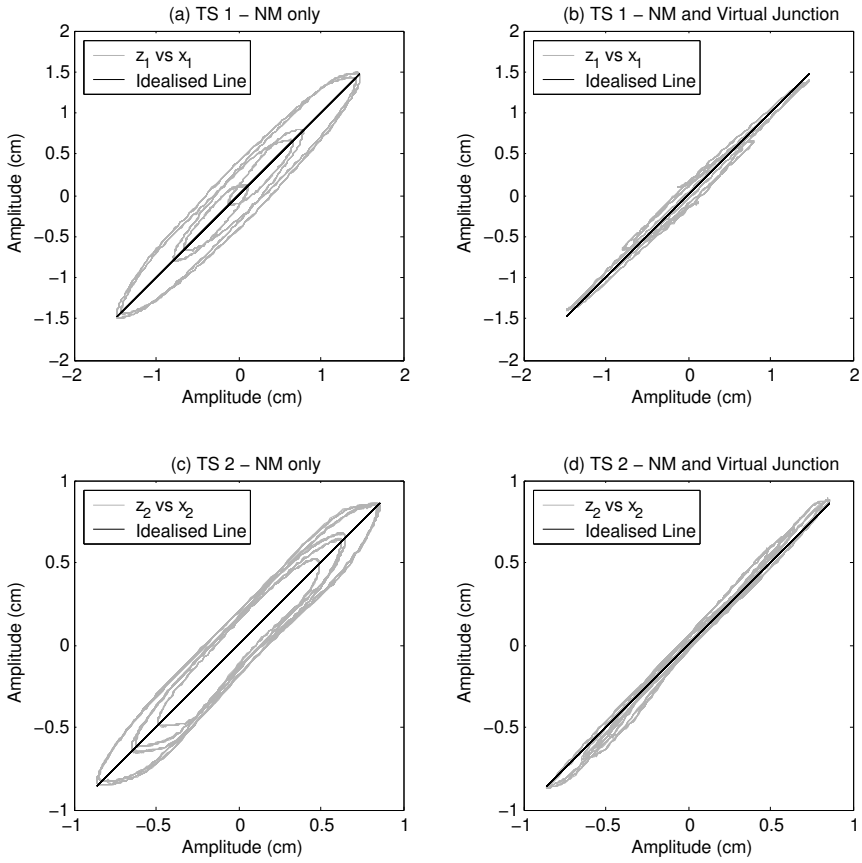

Figure 14. Wall excitation of $r_1 = 3Hz$ and $r_2 = 5Hz$.

systems. Comparing the shape of the subspace plots (a) and (c) we can see that although the transfer systems are the same type of actuator they have slightly differing mechanical properties due to differing frictional characteristics as predicted by the transfer system identification in Section 5.1. This is why we must use a separate model for each transfer system in its respective virtual junctions to account for these mechanical variations.

The transfer system models are found though the system identification process as described in Section 5.1 and are fixed throughout the test procedure. This effectively makes the phase inversion part

of the control algorithm a feed-forward process, which means that the plant cannot not be subject to frequency dependant behaviour. Figure 14 shows the results when the wall excitations are not equal and opposite, thus the transfer systems must now be controlled to a compound sinusoid. We can see from (b) and (d) that again the inclusion of the virtual junction has a beneficial effect on the synchronisation compared to when just the simple numerical model is used, (a) and (c), but not to such a same extent as in Figure 13. This is due to the the transfer system models loosing coherence at the low frequencies. We can also see this when we introduce a sinusoidal sweep as the wall inputs. Figure 15 shows the case where we have a sweep from $1Hz$ to $5Hz$ for the left hand wall excitation, r_1, and a sweep from $3Hz$ to $4Hz$ for the right hand wall excitation, r_2. Although we again see a much higher level of synchronisation when the virtual junction is included in the numerical model, (b) and (d), we cannot achieve the high level of coherence as seen from Figure 13, again due to the frequency dependent characteristics of the transfer systems.

We can see from these results that the phase inversion achieved by the virtual junction has a significant effect on increasing the synchronisation of the transfer systems. However, to increase its effectiveness over the whole plant frequency range the transfer system models could be replaced by an on-line system identification. This would close the control loop round the phase inversion stage of the virtual junction and make the it possible to achieve high levels of synchronisation for compound sinusoids caused by out of phase wall excitations.

6. Conclusions

A bond graph approach to real-time numerical-physical substructuring has been introduced which not only gives new insight into substructuring but also provides a solution to the problem of synchronising the numerical and physical substructures.

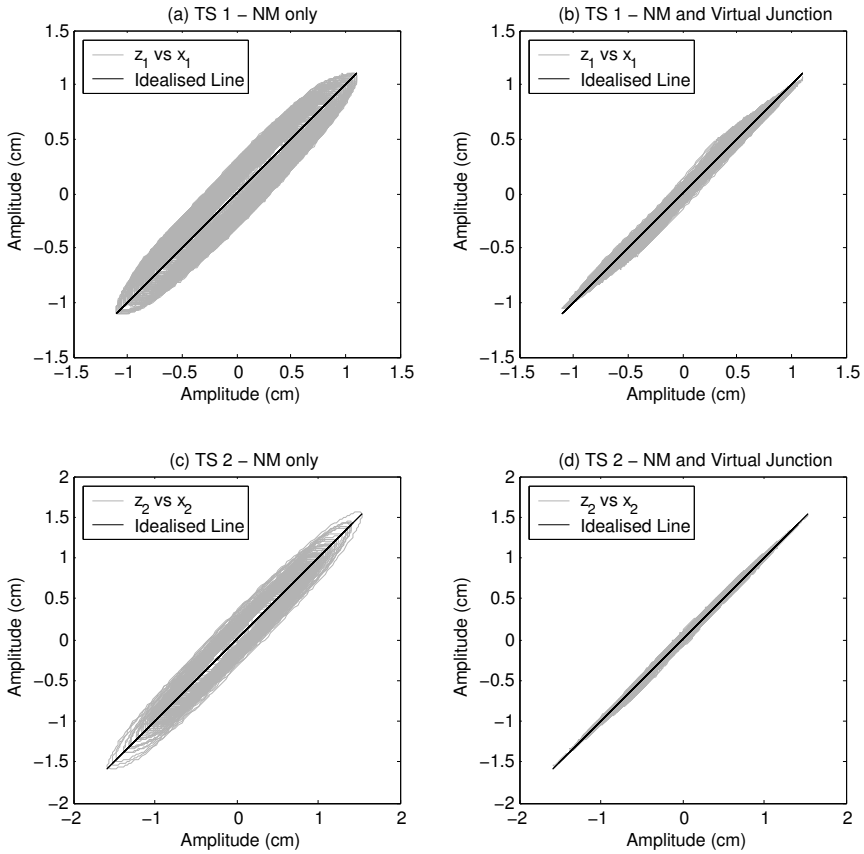

Figure 15. Wall sine sweep excitation of r_1 = 1 to 5Hz and r_2 = 3 to 4Hz in 60 seconds.

The experimental results highlighted the need for an accurate model of the transfer system. Three techniques were used to achieve this: feedback control to reduce non-linearity and the effect of poorly-known parameters; bond graph modelling to give physical insight and system identification to tune physical parameters.

There are a number of topics that will be the subject of further investigation by the authors:

Transfer system design In the light of the experiments reported here, future work will pay close attention to the design transfer system and associated control system. In particular the use of non-

linear modelling and control system design will be investigated. Once again, the bond graph approach can be used not only for modelling and control design but also for actuator sizing [31, 32, 33].

Virtual sensors Sections 2 and 4 assumes that the output of the physical system (in this case F_P) is available for measurement. If this is not the case, or the measurement is badly corrupted by noise, then the *virtual sensor approach* may be used. This has been previously used in the context of Physical Model Based Control [4, 34] and is based on the bond graph analogue to an observer or Kalman filter[35].

Backstepping The relation between the bond graph approach and the backstepping approach of Krstic et al. [36] was noted by [37, 38]. The relationship with the virtual actuator approach is noted by [6, 7]. A non-bond graph approach based on backstepping is therefore a possibility.

On-line System Identification The Experimental validation section, 5.2, highlights the need for the models of the transfer systems to be calculated in an on-line system identification procedure. If this can be achieved as part of the numerical model stage then frequency dependent behaviour and changing plant conditions could be effectively controlled.

Non-Linear Substructure The ability to test to non-linear substructures would enable more realistic structures to be investigated moving towards real industrial applications. Additionally, a non-linear substructure will highlight the difficulties experienced due to cross-coupling between the transfer systems in multi degree of freedom substructuring.

ACKNOWLEDGEMENTS

Two authors would like to acknowledge the support of the EPSRC: Max Wallace is supported via an EPSRC DTA

and David Wagg via an EPSRC Advanced Research Fellowship. Geraint Bevan (Glasgow University) wrote the s-function generation code for MTT.

references

[1] D.J. Wagg and D.P. Stoten. Substructuring of dynamical systems via the adaptive minimal control approach. *Earthquake Engng Struc. Dyn.*, 30(6):865–877, June 2001.

[2] A. P. Darby, A. Blakeborough, and M. S. Williams. Improved control algorithm for real-time substructure testing. *Earthquake Engng Struc. Dyn.*, 30(3):431–448, March 2001.

[3] A. Sharon, N. Hogan, and D. E. Hardt. Controller design in the physical domain. *Journal of the Franklin Institute*, 328(5):697–721, 1991.

[4] P. J. Gawthrop. Physical model-based control: A bond graph approach. *Journal of the Franklin Institute*, 332B(3):285–305, 1995.

[5] Des J. Costello and Peter J. Gawthrop. Physical-model based control: Experiments with a stirred-tank heater. *Trans. IChemE, Part A*, 27:361–370, March 1997.

[6] Peter J Gawthrop, Donald J Ballance, and Dustin Vink. Bond graph based control with virtual actuators. In Norbert Giambiasi and Cluadia Frydman, editors, *Proceedings of the 13th European Simulation Symposium: Simulation in Industry*, pages 813–817, Marseille, France, October 2001. SCS. ISBN 90-77039-02-3.

[7] Peter J Gawthrop. Bond graph based control using virtual actuators. *Proceedings of the Institution of Mechanical Engineers Pt. I: Journal of Systems and Control Engineering*, 218(4):251–268, September 2004. URL http://dx.doi.org/10.1243/0959651041165864.

[8] M. Nakashima, H. Kato, and E. Takaoka. Development of real-time pseudo dynamic testing. *Earthquake Engineering and Structural Dynamics*, 21:779–92, 1992.

[9] J. Donea, P. Magonette, P. Negro, P. Pegon, A. Pinto, and G. Verzeletti. Pseudodynamic capabilities of the elsa laboratory for earthquake testing of large structures. *Earthquake Spectra*, 12(1):163–180, 1996.

[10] Yu-Yuan Lin, Kuo-Chun Chang, and Yuan-Li Wang. Comparison of displacement coefficient method and capacity spectrum method with experimental results of rc columns. *Earthquake Engineering and Structural Dynamics*, 33(1):35–48, 2004.

[11] M. S. Williams and A. Blakeborough. Laboratory testing of structures under dynamic loads: an introductory review. *Philosophical Transactions of the Royal Society A*, 359:1651 – 1669, 2001.

[12] A. Blakeborough, M. S. Williams, A. P. Darby, and D. M. Williams. The development of real-time substructure testing. *Philosopical Transactions of the Royal Society of London A*, 359:1869–1891, 2001.

[13] A. P. Darby, A. Blakeborough, and M. S. Williams. Real-time substructure tests using hydraulic actuator. *Journal of Engineering Mechanics*, 125(10):1133–1139, 2001.

[14] M. I. Wallace, D. J. Wagg, and S. A. Neild. A polynomial based forward prediction algorithm for improving the accuracy of real-time dynamic substructuring. *Submitted to Proceedings of the Royal Society A*, 2004.

[15] H. M. Paynter. *Analysis and design of engineering systems*. MIT Press, Cambridge, Mass., 1961.

[16] Peter J Gawthrop and Serge Scavarda. Special issue on bond graphs: Editorial. *Proceedings of the Institution of Mechanical Engineers Pt. I: Journal of Systems and Control Engineering*, 216(I1):i–v, March 2002. URL http://dx.doi.org/10.1243/0959651021541363.

[17] Dean Karnopp, Donald L. Margolis, and Ronald C. Rosenberg. *System Dynamics : Modeling and Simulation of Mechatronic Systems*. Horizon Publishers and Distributors Inc, 3rd edition, January 2000.

[18] Amalendu Mukherjee and Ranjit Karmakar. *Modelling and Simulation of Engineering Systems through Bondgraphs*. Alpha Science, 2000.

[19] P. J. Gawthrop and L. P. S. Smith. *Metamodelling: Bond Graphs and Dynamic Systems*. Prentice Hall, Hemel Hempstead, Herts, England., 1996. ISBN 0-13-489824-9.

[20] Lennart Ljung and Torkel Glad. *Modeling of Dynamic Systems*. Prentice Hall, 1994.

[21] F. E. Cellier. *Continuous system modelling*. Springer-Verlag, 1991.

[22] W. Algaard, A. Agar, and N. Bicanic. Enhanced integral form of the Newmark time stepping scheme for pseudodynamic testing. *Engineering Computations*, 18(3):676–689, 2001.

[23] T. Horiuchi, M. Inoue, T. Konno, and Y. Namita. Real-time hybrid experimental system with actuator delay compensation and its application to a piping system with energy absorber. *Earthquake Engineering and Structural Dynamics*, 28:1121–1141, 1999.

[24] Toshihiko Horiuchi and Takao Konno. A new method for compensating actuator delay in real-time hybrid experiments. *Philosophical Transactions of the Royal Society A*, 359:1893 – 1909, 2001.

[25] MTT. MTT: Model transformation tools. Online WWW Home Page, 2002. URL: http://mtt.sourceforge.net.

[26] P.C. Sen. *Principles of Electrical Machines and Power Electronics*. John Wiley, 2nd edition, 1997.

[27] L Wang and W R Cluett. *From Plant Data to Process Control*. Taylor and Francis, London and New York, 2000.

[28] Peter J Gawthrop. Physically-plausible models for identification. In *Proceedings of the 2003 International Conference On Bond Graph Modeling and Simulation (ICBGM'03)*, Simulation Series, Orlando, Florida, U.S.A., January 2003. Society for Computer Simulation.

[29] Peter J Gawthrop. Sensitivity bond graphs. *Journal of the Franklin Institute*, 337(7):907–922, November 2000. URL http://dx.doi.org/10.1016/S0016-0032(00)00052-1.

[30] P. Ashwin. Non-linear dynamics, loss of synchronization and symmetry breaking. *Proceedings of the Institution of Mechanical Engineers, Part G: Journal of Aerospace Engineering*, 212(3):183–187, 1998.

[31] Roger F Ngwompo and Peter J Gawthrop. Bond graph based simulation of nonlinear inverse systems using physical performance specifications. *Journal of the Franklin Institute*, 336(8):1225–1247, November 1999. URL http://dx.doi.org/10.1016/S0016-0032(99)00032-0.

[32] Ngwompo R F, Scavarda S, and Thomasset D. Physical model-based inversion in control systems design using bond graph representation part 1: theory. *Proceedings of the I MECH E Part I Journal of Systems and Control Engineering*, 215(2):95–103, April 2001.

[33] Ngwompo R F, Scavarda S, and Thomasset D. Physical model-based inversion in control systems design using bond graph representation part 2: applications. *Proceedings of the I MECH E Part I Journal of Systems and Control Engineering*, 215(2):105–112, April 2001.

[34] Peter J. Gawthrop and Donald J. Ballance. Symbolic algebra and physical-model-based control. *Computing and Control Journal*, 8(2):70–76, April 1997. ISSN 0956-3385.

[35] D. C. Karnopp. Bond graphs in control: Physical state variables and observers. *J. Franklin Institute*, 308(3): 221–234, 1979.

[36] M. Krstic, I. Kanellakopoulos, and P. V. Kokotovic. *Nonlinear and Adaptive Control design*. New York: Wiley, 1995.

[37] T-J Yeh. Backstepping design in the physical domain. In *Proceedings of the American Control Conference*, 1999.

[38] T-J Yeh. Backstepping control in the physical domain. *Journal of the Franklin Institute*, 338:455–479, 2001.